Hydrogenolysis of Glycerol to Monoalcohols over Supported Mo and W Catalysts

Mzamo L. Shozi,[†] Venkata D. B. C. Dasireddy,[†] Sooboo Singh,[†] Pheladi Mohlala,[‡] David J. Morgan,[§] and Holger B. Friedrich[*,†]

[†]School of Chemistry and Physics, University of KwaZulu-Natal, Durban 4000, South Africa

[‡]Sasol South Africa (Pty) Ltd, Group Technology R&T, 1 Klasie Havenga Street, Sasolburg 1974, South Africa

[§]Cardiff Catalysis Institute, Cardiff University, Main Building, Park Place, Cardiff CF10 3AT, United Kingdom

[*] Supporting Information

ABSTRACT: MoO_3 and WO_3 were supported on γ-Al_2O_3 and SiO_2 with nominal loadings of 10 wt % via wet impregnation. The catalysts were characterized using XRD, TPR, Pulse TPD, Raman, TEM, and BET surface area. The alumina supported catalysts were found to contain higher Brønsted acidity compared to those supported on silica. These catalysts were evaluated in the hydrogenolysis of glycerol in a continuous flow fixed bed reactor in a temperature range of 250−325 °C and a H_2 pressure of 60 bar. All catalysts were active, with activity increasing with temperature as well as Brønsted acidity. The selectivity to ethylene glycol and 1,2-propanediol decreased with increase in temperature. In parallel, the selectivity to lower alcohols such as methanol, ethanol, 2-propanol, and 1-propanol increased with temperature as the ethylene glycol and 1,2-propanediol reacted further to these products due to C−C bond cleavage. The total selectivity to lower alcohols was 34.6, 64.8, 70.6, and 54.6% over Mo/Al_2O_3, Mo/SiO_2, W/Al_2O_3, and W/SiO_2 respectively. The total selectivity to lower alcohols increased to 73.6, 72.8, 85.3, and 66.1% over Mo/Al_2O_3, Mo/SiO_2, W/Al_2O_3, and W/SiO_2 respectively when the H_2:glycerol ratio was doubled.

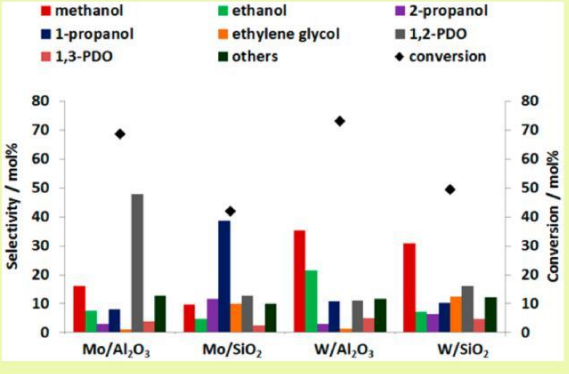

KEYWORDS: Supported catalysts, Molybdenum, Tungsten, Glycerol, Hydrogenolysis, Lower alcohols

INTRODUCTION

The expansion of the biodiesel industry has led to an oversupply of glycerol, the major byproduct of biodiesel production. Glycerol is thus a cheap, large-volume feedstock, and the need for new applications for it has risen. The production of lower alcohols is of industrial interest since ethanol is a renewable fuel and fuel additive, and methanol and 1-propanol are used as solvents in the paint and cosmetic industries.[1] 1,2-Propanediol (1,2-PDO) and ethylene glycol (EG) which are also formed during this process have an important use as antifreeze liquids and additives in liquid detergent.[2−4] One of the processes that has potential in obtaining these lower alcohols from glycerol is hydrogenolysis.[5−9] Platinum group metals are the most effective catalysts in hydrogenolysis;[10−18] however, they are very expensive and can only be used in small amounts. Therefore, the use of metals such as molybdenum and tungsten could provide a cost-effective hydrogenolysis process.

Glycerol hydrogenolysis over tungsten catalysts has received much attention over the past few years.[4,10,11,19−30] Kurosaka et al.[19] reported the use of supported WO_3 catalysts doped with 2 wt % Pt for the conversion of glycerol to 1,3-propanediol (1,3-PDO). The $Pt/WO_3/ZrO_2$ catalyst gave the highest yield of the diol at 24%. Gong et al.[20] showed that the use of a $Pt/WO_3/TiO_2/SiO_2$ catalyst could convert glycerol to 1,3-PDO in water medium, with a glycerol conversion of 15% and selectivity to the diol of 50.5%. Lui et al.[11] developed a mesoporous WO_3 supported Pt catalyst which showed a conversion of 18% and a selectivity to 1,3-PDO of 39%. Zhu et al.[21] developed a bifunctional catalyst, $Pt−H_4SiW_{12}O_{40}/ZrO_2$, which displayed good performance with a glycerol conversion of 85% and selectivity to 1-propanol and 1,3-PDO of 62 and 22% respectively. When the weight hourly space velocity (WHSV) was doubled under the same conditions of temperature and pressure, the conversion dropped to 24% and selectivity to 1-propanol and 1,3-PDO was 22 and 48% respectively.[22] Under the same conditions previously reported,[22] Zhu et al.[23] showed that the addition of alkaline metals such as Li, K, Rb, and Cs could tune the acidic property of the tungsten heteropolyacid and control the activity in glycerol hydrogenolysis, giving a selectivity as high as 54% to 1,3-PDO with Li. Silica modified $Pt/WO_x/ZrO_2$ catalysts for the selective hydrogenolysis of

glycerol to 1,3-PDO have also been reported.[28] Incorporation of SiO_2 led to an increase in activity and selectivity to 1,3-PDO reaching a maximum of 60.8% when the SiO_2 loading was 5 wt %.

Supported molybdenum catalysts in the hydrogenolysis of glycerol have also been reported.[12,13,30,31] Koso et al.[12] reported a Rh-MoO_x/SiO_2 catalyst of hydrogen pressure at 8.0 MPa and a reaction temperature of 393 K, to give 1,3-PDO, 1,2-PDO, 1-propanol, and 2-propanol, with the selectivity to 1,2-PDO being the highest at 41%. Liao et al.,[13] on the other hand, used Mo as a modifier for Ru/SiO_2 catalysts in the hydrogenolysis of glycerol. The reactions were carried out in a continuous flow fixed bed reactor using an ambient hydrogen pressure and a molar ratio of H_2:glycerol of 185:1. Using Mo drastically reduced the activity due to the strong interaction between Mo and Ru which suppressed the activity of Ru. The yield to C3 products (acetol, 1,2-PDO, and 1-propanol) increased from 11.8%, when using bare Ru/SiO_2, to 23.6% when Mo was added. Mo catalysts have also been used in the hydrogenolysis of 4-(1-naphthylmethyl)bibenzyl,[32] n-butane,[33,34] and tetrahy-drofurfuryl alcohol.[35] Here we report supported Mo and W catalysts in the hydrogenolysis of glycerol and the effect of temperature and H_2 content on the conversion of glycerol and selectivities to monoalcohols under continuous flow conditions.

EXPERIMENTAL SECTION

Catalyst Preparation. The supported MoO_3 and WO_3 catalysts were prepared by impregnating the supports (γ-Al_2O_3 and SiO_2, Alfa-Aesar) with an aqueous solution of $(NH_4)_6Mo_7O_{24}{\cdot}4H_2O$ and $(NH_4)_6H_2W_{12}O_{40}{\cdot}xH_2O$, respectively, to obtain a nominal loading amount of 10 wt % MoO_3 and 10 wt % WO_3. After impregnation, the catalysts were dried at 110 °C for 12 h, followed by calcination in air at 550 °C for 8 h.

Catalyst Characterization. The BET surface area and pore volume measurements were carried out using a Micrometrics Tristar II Surface area and Porosity Analyzer. Prior to analysis, samples were weighed and degassed at 200 °C overnight under constant flow of nitrogen gas. In order to determine metal loading on the support, inductively coupled plasma analysis was performed using a PerkinElmer Optical Emission Spectrometer Optima 5300 DV. Prior to analysis, samples were digested in acid and then diluted accordingly. Standards were prepared from 1000 ppm metal stock solutions purchased from Fluka. Powder X-ray diffraction (XRD) studies were conducted on a Bruker D8 Advance diffractometer with Cu ($K\alpha$, λ = 1.5406 Å) as the radiation source.

Temperature-programmed reduction (TPR) analyses were carried out using a Micromeritics Autochem 2920 chemisorption analyzer. Prior to reduction approximately 50 mg of the sample was placed in a U-shaped quartz tube. The sample was dried by heating at 5 °C/min under helium flow (50 mL/min) to 120 °C and kept at this temperature for 10 min. The sample was then cooled to room temperature and subsequently heated again at 10 °C/min under 10% H_2/Ar flow (50 mL/min) to 1000 °C and kept at this temperature for 10 min. The water formed during reduction was trapped using a dry ice/isopropyl alcohol bath. The amount of hydrogen consumed during reduction was measured with the TCD. Pulse chemisorption-TPD-MS studies were carried out on a Micromeritics Autochem 2920 chemisorption analyzer coupled with Cirrus Mass Spectrometer to study the Brønsted acid sites on the prepared catalysts. Approximately 50 mg of sample was placed in a quartz U-tube containing quartz wool, fitted with a thermocouple for continuous temperature measurements. The sample was activated first by heating to 550 °C at 10 °C/min in an inert helium environment and then cooling to 100 °C, the adsorption temperature. The activation of the samples was followed by pulse chemisorption. During this step, 30 injections of propylamine vapor were dosed onto the catalyst by means of an inert gas, helium, flowing through a 1 cm^3 loop. The last part of the analysis involved a temperature-programmed desorption (TPD). At this step in the analysis, the mass spectrometer (MS) began scanning for propylene, the product of interest. Data were collected during a temperature ramp from 100 to 550 °C. The mass spectrometer is calibrated using a standard propylene (5%) in He gas. The total acidity is calculated by using a deconvolution of propylamine pulse area.

Raman spectroscopy was carried out using an Advantage 532 series spectrometer (NIR Spectrometer) utilizing Nuspec software. The surface morphology of the catalysts was observed using a Zeiss Ultra plus Field Emission Gun microscope. The images were captured using SmartSEM software. Prior to SEM analysis, the samples were mounted on aluminum stubs using double-sided carbon tape and subsequently gold spluttered using the Polaron SC500 coating unit. Transmission electron microscopy (TEM) images were viewed using a Jeol JEM-1010 Electron Microscope. The images were captured and analyzed using iTEM software. Prior to analysis, the samples were sonicated in ethanol after which they were placed on a copper grid. XPS data was acquired on a Thermo-Fisher Scientific K-Alpha$^+$ X-ray photoelectron spectrometer, utilizing monochromatic Al $K\alpha$ radiation operating at a power of 72 W (6 mA × 12 kV). High resolution scans were performed at a pass energy of 40 eV, with a 0.1 eV step, while survey spectra were acquired at a pass energy of 150 eV and a step size of 1 eV. Charge neutralization was achieved using a combination of low energy electrons and argon ions which gave a reproducible C(1s) binding energy of 284.8 eV for all samples.

Catalytic Testing. Catalytic testing was carried out using a continuous flow fixed-bed reactor comprising of a reactor tube with a length of 250 mm and an internal diameter of 20 mm. The catalysts were pelletized and sieved to a mesh size range of 300−600 μm. A catalyst volume of 3 mL was mixed with an equal amount of 24-grit carborundum and loaded in the reactor tube. The GHSV of hydrogen was maintained at 1860 h^{-1} and the LHSV of glycerol at 10 h^{-1} for all reactions. Reactions were carried out between 250−325 °C at a hydrogen pressure of 60 bar. Prior to testing, the catalysts were reduced under hydrogen, Mo catalysts at 450 °C and W catalysts at 550 °C, after which the reactor was cooled to operating temperatures where Mo and W were in the metallic state. The liquid products and unreacted glycerol were collected in a catchpot cooled to −10 °C and analyzed on a PerkinElmer Clarus 500 GC equipped with an FID and a PONA column. The gas samples were collected and analyzed for methane and carbon oxides on a PerkinElmer Clarus 400 GC equipped with a TCD. Mass balances were 100 ± 5% on a carbon basis. Conversion and product selectivities were reported with a ±2% error. Only trace amounts of "heavy" products were observed.[36]

RESULTS AND DISCUSSION

Catalyst Characterization. Physical Properties. The textural and physical properties are shown in Table 1. When the metal oxide is impregnated onto the support, the surface areas and pore volumes decrease. This is due to the metal oxide covering the surface of the support as well as blocking the pores of the support, reducing nitrogen accessibility. The surface area of the supports decreased by approximately 40−50% when the metal oxides were incorporated.

Table 1. Physical and Textural Properties of the Catalysts

	metal content/wt %			
catalyst	Mo	W	BET surface area/ $m^2\ g^{-1}$	pore volume/ $cm^3\ g^{-1}$
Al_2O_3			216	0.65
SiO_2			155	0.66
Mo/Al_2O_3	9.54		105	0.34
Mo/SiO_2	9.34		71	0.25
W/Al_2O_3		9.32	92	0.25
W/SiO_2		9.21	63	0.20

X-ray Diffraction. The X-ray diffractograms of the catalysts are shown in Figure 1, and the sharp peaks show that they are

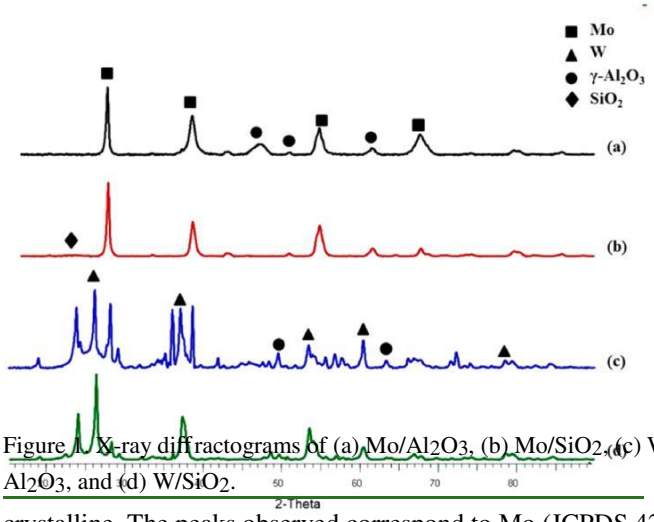

Figure 1. X-ray diffractograms of (a) Mo/Al_2O_3, (b) Mo/SiO_2, (c) W/Al_2O_3, and (d) W/SiO_2.

crystalline. The peaks observed correspond to Mo (JCPDS 42-1120)[37] and W (JCPDS 04-0806)[38] formed via in situ reduction in the reactor. The characteristic peaks for Al_2O_3 were also observed with the characteristic peak for SiO_2 at ~22° overlapping with the metal oxide peaks for both Mo and W. For the W catalysts there are some oxide phases present since tungsten is difficult to reduce.[39]

Temperature-Programmed Reduction. Figure 2 shows the TPR profiles of the catalysts, and a summary of the results with reduction temperatures and degree of reducibility is shown in Table 2. The TPR profile of Mo/Al_2O_3 exhibits three reduction peaks at temperatures of 488, 613, and 781 °C. In general, the reduction of molybdenum species follows the pathway below as reported:[40,41]

$$MoO_3 + H_2 \rightarrow MoO_2 + H_2O \quad (1)$$

$$MoO_2 + H_2 \rightarrow Mo^0 + 2H_2O \quad (2)$$

Reaction 1, the reduction process of MoO_3 to MoO_2, occurs over a temperature range of 450−650 °C. Reaction 2 occurs at a temperature range of 650−800 °C and is assigned to the reduction of MoO_2 to molybdenum metal.[42] For the catalyst Mo/Al_2O_3, due to the strong and weak interactions with the support, the reduction profile showed three peaks and the reduction of strongly bound MoO_3 occurred at higher temperatures when compared to the weakly bound MoO_3.

Table 2. Summary of TPR Data of the MoO_3 and WO_3 Catalysts

catalyst	peak 1/°C	peak 2/°C	peak 3/°C	degree of reducibility/%
Mo/Al_2O_3	488	613	781	81.3
Mo/SiO_2	450	641	701	69.8
W/Al_2O_3	586	837		79.4
W/SiO_2	574	790	905	60.8

The first peak at 488 °C exhibits the reduction of loosely bound MoO_3 on alumina and the first reduction of MoO_3 on γ-alumina usually occurs in the range 360−560 °C.[43,44] The presence of loosely bound molybdenum oxides might be due to the preparation method of the catalysts.[40] The second peak at 613 °C can be assigned to the reduction of strongly bound MoO_3 to MoO_2, and the third peak can be assigned to the further reduction of MoO_2 to molybdenum metal. A similar pattern is also observed for MoO_3 supported on silica. Mo/SiO_2 also showed three peaks in the TPR profile, indicating that the reduction of molybdenum oxide also occurred in three steps. The reduction of loosely bound MoO_3 can be assigned to the peak at 450 °C. The reduction of MoO_3 to MoO_2 and the further reduction of MoO_2 to molybdenum metal can be observed from peaks at temperatures of 641 and 701 °C respectively. The reduction of MoO_3 supported on silica occurred at lower temperatures in comparison to the MoO_3 supported on alumina. This could be due to the weaker interaction of MoO_3 with silica compared to the interaction of MoO_3 supported on alumina.[45] Mo/Al_2O_3 and Mo/SiO_2 showed a degree of reducibility of 81% and 70% respectively. Thus, it can be concluded that the MoO_3 in both the catalysts is not totally reduced to molybdenum metal.

In general, the reduction of WO_3 follows the pathway shown by eqs 3 and 4 which is similar to the reduction profile of MoO_3:[46,47]

$$WO_3 + H_2 \rightarrow WO_2 + H_2O \quad (3)$$

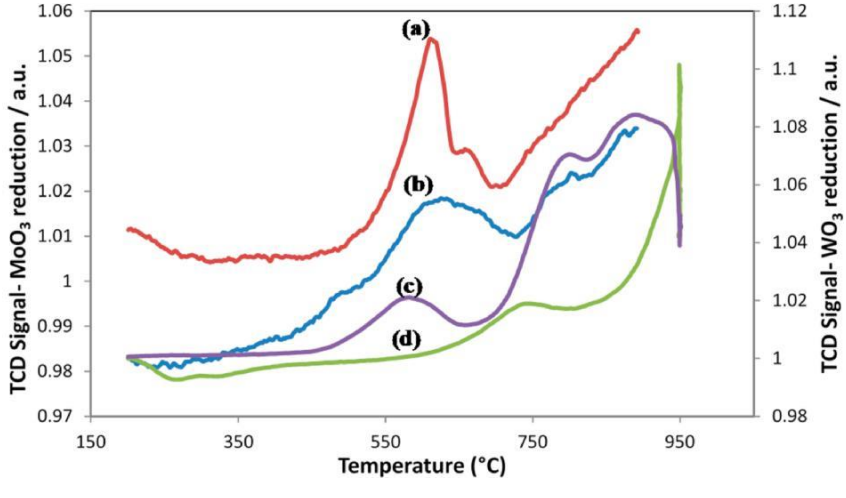

Figure 2. TPR profiles of (a) Mo/SiO_2, (b) Mo/Al_2O_3, (c) W/SiO_2, and (d) W/Al_2O_3 catalysts.

$$WO_2 + H_2 \rightarrow W + 2H_2O \quad (4)$$

Reaction 3 is the reduction of WO_3 to WO_2 which occurs over a temperature range of 400−600 °C. Reaction 4 occurs at a temperature range of 600−800 °C and is assigned to the reduction of WO_2 to tungsten metal. Due to the interaction of WO_3 with silica, the reduction of WO_3 to tungsten metal occurs in three reduction steps as seen in the TPR profile. The first peak at 574 °C is generally attributed to the reduction of loosely bounded WO species on silica.[40] The second peak at 790 °C can be assigned to the reduction of strongly bounded WO_3 to WO_2, and the third peak at 905 °C can be assigned to the further reduction of WO_2 to tungsten metal.

In contrast, the reduction of WO_3 on the alumina exhibited only two peaks. Similar observation were also made by Vermaire and Berge,[48] who observed the reduction of WO_3 supported on titania and alumina. This could be due to two reasons: (a) weak interaction of WO_3 with alumina[47,48] and (b) presence of W−O−W species as observed in Raman (Figure S2).[49] The weak interaction of WO_3 with alumina could be due to the supporting of acidic WO_3 on the amphoteric alumina.[46] Thus, due to the weak interaction, the reduction of WO_3 occurs in only two reduction steps. The reduction of W−O−W occurs at lower temperatures compared to the reduction of O W O species which exist when WO_3 is supported on silica and zirconia.[46,49] In the reduction profile of WO_3/Al_2O_3, the first peak at 586 °C can be attributed to the reduction of weakly bound WO_3 to WO_2, and the peak at 837 °C can be attributed to the reduction of WO_2 to tungsten metal.[49] WO_3/Al_2O_3 and WO_3/SiO_2 showed degrees of reducibility of 80% and 61% respectively. It can be concluded that the WO_3 in both the catalysts is not reduced totally to tungsten metal. Similar observations were also made with the MoO_3 catalysts which could be due to the low concentration of the reductant (5% H_2 in Ar) used for the reduction.

Temperature-Programmed Desorption. The TPD profiles can be seen in Figure S1, and the total acidity determined is shown in Table 3. The TPD profiles of the catalysts revealed the existence of weak (<300 °C) and strong acidic sites (>300 °C) on all the catalysts. In the case of the Mo catalysts, the Brønsted acidity is likely due to the presence of Mo which has been reported to exhibit maximum acidity at a loading of ~11 wt %.[50,51] The Brønsted acidity is caused by the hydroxyl groups formed on the molybdenum oxide monolayer domain and Mo; Mo−OH or Mo−(OH)−Mo function as Brønsted acidic sites.[51]

Table 3. Total Brønsted Acidity of the Mo and W Catalysts Determined from Isopropyl Amine TPD

catalyst	total Brønsted acidity/μmol g^{-1}
Mo/Al_2O_3	10.15
Mo/SiO_2	1.79
W/Al_2O_3	10.31
W/SiO_2	2.47

For the W catalysts, W/Al_2O_3 had a higher Brønsted acidity than W/SiO_2, and similar observations were made by Mitran et al.[52] It has been reported that for W/SiO_2 catalysts, SiO_2 possesses minimal acidity and W is responsible for the acid sites due to the hydroxyl groups that are formed by protonating the bridging Si−O−W or terminal W−O bonds on the surface Brønsted acidity due to the reducible WO_x domains which are acting as redox sites required for the formation of H^+ species from H_2, and this also contributes to the total acidity even at low loadings of tungsten.[10,53]

Raman Spectroscopy. Figure S2 shows the Raman spectra of the Mo and W catalysts. The Mo catalysts showed a band at ~1000 cm^{-1} which is assigned to the Mo O stretching vibration mode due to polymolybdate species. The bands at ~820 and ~680 cm^{-1} are due to crystalline MoO_3 and also indicate that part of the Mo is not well dispersed on the support.[54−57] The band at ~320 cm^{-1} for both the Mo catalysts is assigned to the Mo−O−Mo bending mode.[58] For Mo/Al_2O_3, the bands at ~380 cm^{-1} are assigned to bending modes of the terminal Mo O bond.[44] The W catalysts showed bands at ~800 and ~700 cm^{-1} which are characteristic of the stretching and bending vibrations of W−O−W respectively. These two bands are also characteristic of crystalline WO_3.[59−61] For the W/SiO_2 catalyst, a band at ~273 cm^{-1} is indicative of the deformation mode of W−O−W, and a band at ~326 cm^{-1} is due to crystalline WO_3.[60,61]

X-ray Photoelectron Spectroscopy. Figure S3 shows the W(4f) and Mo(3d) core-level spectra for each catalyst. For the tungsten based catalysts, there is a clear difference in the distribution of tungsten oxidation states for each support. For the alumina supported tungsten catalyst, the spectrum is dominated by WO_3 species (35.9 eV), although WO_2 (32.9 eV) and WO_x (34.4 eV) are also present, together with a very small percentage of metallic W (30.6 eV). These species are also in agreement with observations made in TPR. The exact oxidation state of the species at 34.4 eV is unclear; although some researchers assign this as W(5+), we consider it to be substoichiometric WO_3.[62] For WO_3/SiO_2, similar oxidation states are found, but clearly there is a greater concentration of the lower oxidation states.

For the supported molybdenum catalysts the spectra are found to be very similar and comprise of predominantly MoO_2 species (Mo(3d5/2) 229.0 eV), which has a complex line shape due to screened states,[63] together with Mo(5+) and Mo(6+) oxides; a greater percentage of the Mo(5+) is found for the alumina supported catalyst.

Catalytic Testing. Effect of Temperature. Figure 3 shows the effect of temperature on the conversion of glycerol for each of the catalysts. The conversion was found to increase with temperature for all catalysts, as expected, and this is also in agreement with the calculated turnover frequencies in Table S1. The catalysts supported on alumina showed similar conversion due to similar Brønsted acidity. The alumina supported catalysts also showed higher conversion than the silica supported catalysts, likely due to higher Brønsted acidity, their higher surface area, as well as them having a higher degree of reducibility (Tables 1 and 2). Importantly, the catalysts were stable, showing unchanged conversion and selectivity, at each temperature for 24 h.

Figures 4a−d show the effect of temperature on the product selectivities over the different catalysts. The selectivity towards 1,2-PDO and ethylene glycol (EG) decreased, while the selectivity to lower alcohols increased with increasing temperature. This suggests that the lower alcohols are formed via hydrogenolysis of 1,2-PDO and EG. In support of this, lower alcohols were obtained when 1,2-PDO and EG were used as feed in hydrogenolysis over supported Ni catalysts.[64] Similar observations were made by Ueda and co-workers who found

which are evident in Raman (Figure S2). W/Al_2O_3 had higher the selectivity of 1,2-PDO to decrease with increasing

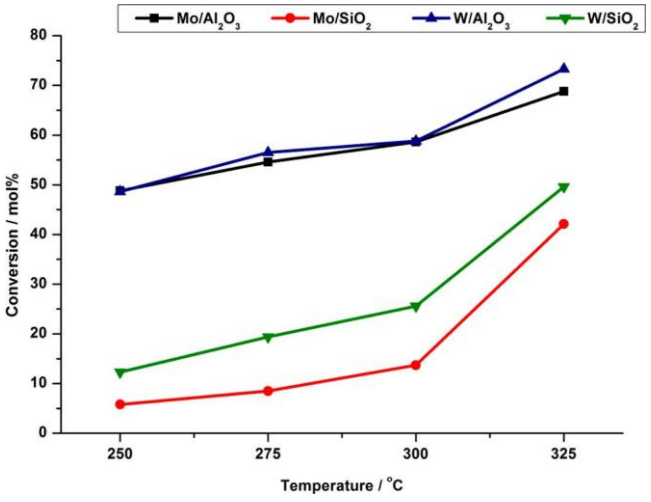

Figure 3. Conversion of glycerol with temperature over the different catalysts. Reaction conditions: 60 wt % glycerol/H_2O, 3 mL catalyst bed, 60 bar H_2.

formation of EG in the hydrogenolysis of glycerol over a Pt-promoted Ni/γ-Al_2O_3 catalyst.[65]

Figure 5 shows the selectivity of the products over the catalysts at 325 °C. This temperature was chosen as it gave the highest conversion and selectivity to lower alcohols for all the catalysts studied. The catalysts showed a higher selectivity to 1,2-PDO than EG and 1,3-PDO, due to higher Brønsted acidity which facilitates the dehydration step which leads to the formation of 1,2-PDO.[6,66,67] Hydrogenolysis of glycerol occurs via acid-catalyzed dehydration to form intermediates (acetol and 3-hydroxypropaldehyde (3-HPA)) and subsequent hydro-genation to form propanediols (1,2-PDO and 1,3-PDO) on metal sites.[5–7] It is well established that metal and acid sites, along with active hydrogen species, enhance glycerol hydro-genolysis. Besides acid strength, the nature of the acidic sites, i.e. Brønsted and Lewis acidic sites, play a predominant role in determining product formation. It is evident that Brønsted acid sites are responsible for 1,3-PDO formation, while Lewis acid sites allow formation of 1,2-PDO.[68]

These observations are based on a reaction mechanism proposed by Priya et al.[68] In this mechanism, the secondary carbocation intermediate to 3-HPA is more stable than the primary carbocation to acetol. Therefore, 3-HPA formation is kinetically more favorable than acetol production, although thermodynamically less stable. This pathway involves the protonation and dehydration of the secondary hydroxyl group of adsorbed glycerol on the Brønsted acid sites of the support by interacting with bridging OH groups of the support. The alkoxy species formed as a result of dehydration desorb,

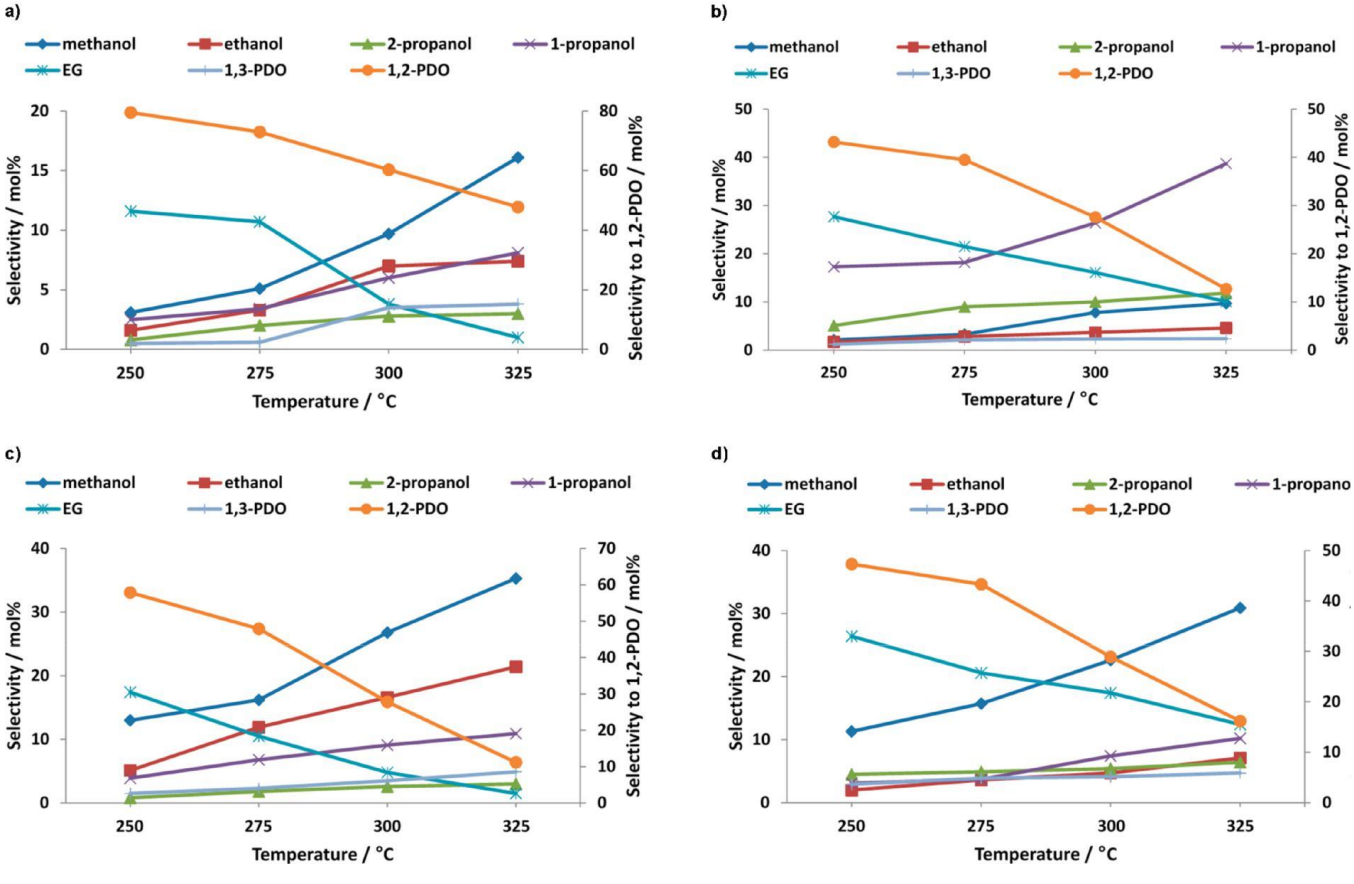

Figure 4. a) Effect of temperature on product selectivity over Mo/Al_2O_3. Reaction conditions: 60 wt % glycerol/H_2O, 3 mL catalyst bed, 60 bar H_2.
Other products: acetol, methane, ethane, propane, CO, CO_2, unknowns. b) Effect of temperature on product selectivity over Mo/SiO_2. Reaction conditions: 60 wt % glycerol/H_2O, 3 mL catalyst bed, 60 bar H_2. Other products: acetol, methane, ethane, propane, CO, CO_2, unknowns. c) Effect of temperature on product selectivity over W/Al_2O_3. Reaction conditions: 60 wt % glycerol/H_2O, 3 mL catalyst bed, 60 bar H_2. Other products: acetol, methane, ethane, propane, CO, CO_2, unknowns. d) Effect of temperature on product selectivity over W/SiO_2. Reaction conditions: 60 wt % glycerol/H_2O, 3 mL catalyst bed, 60 bar H_2. Other products: acetol, methane, ethane, propane, CO, CO_2, unknowns.

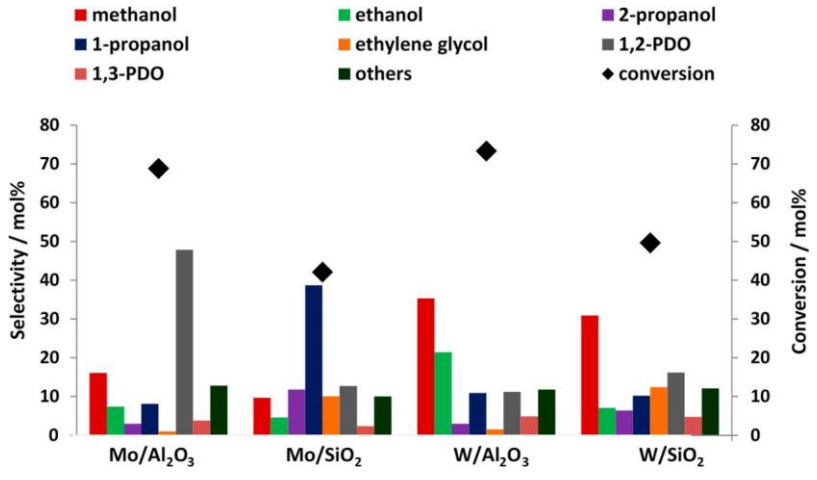

Figure 5. Conversion of glycerol and selectivity to products over the catalysts at 325 °C. Reaction conditions: 60 wt % glycerol/H_2O, 3 mL catalyst bed, 60 bar H_2. Other products: acetol, methane, ethane, propane, CO, CO_2, unknowns.

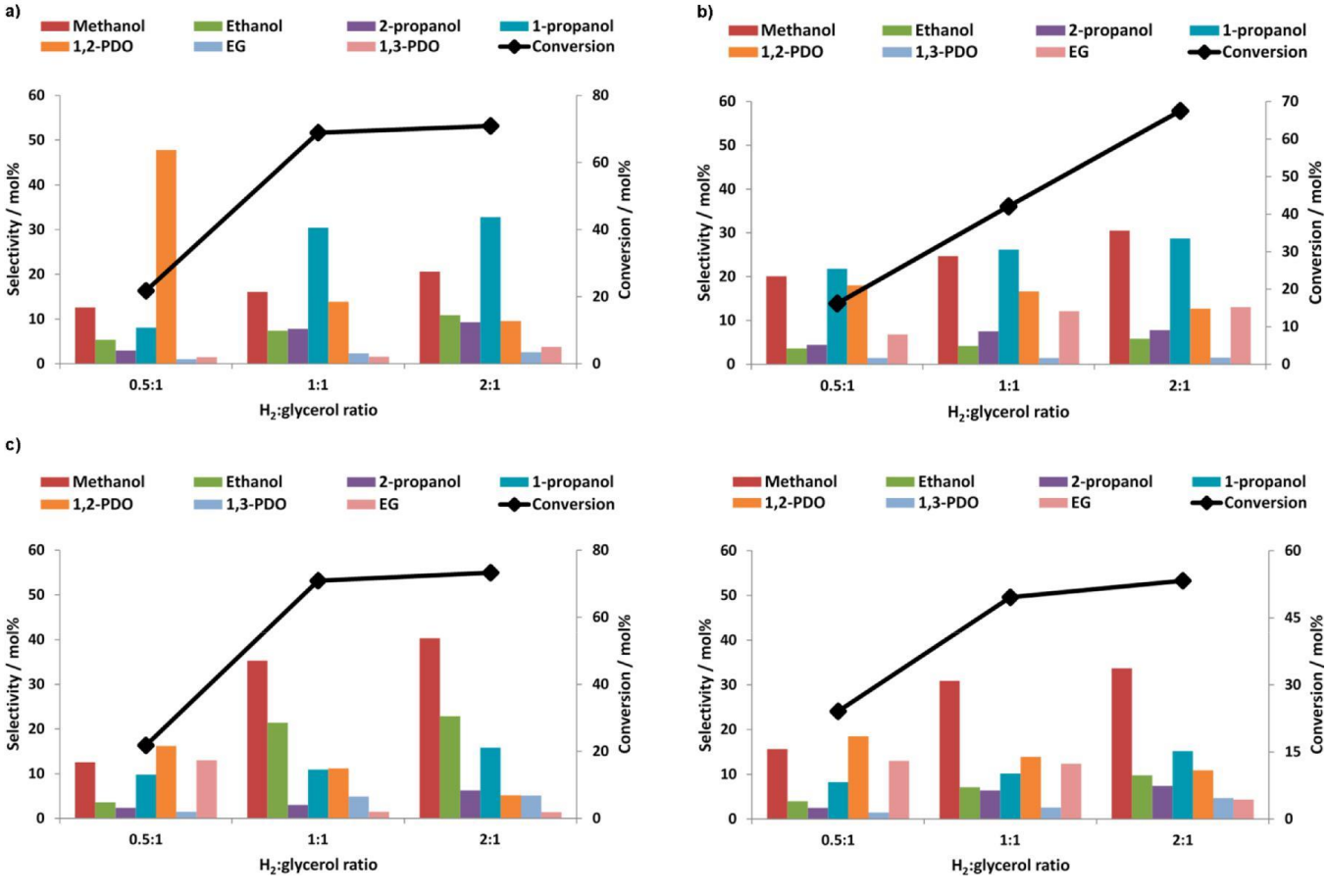

Figure 6. a) Effect of H_2:glycerol ratio on conversion and product selectivity over Mo/Al_2O_3 at 325 °C. Reaction conditions: 60 wt % glycerol/H_2O, 3 mL catalyst bed, 60 bar H_2. Other products: acetol, methane, ethane, propane, CO, CO_2, unknowns. b) Effect of H_2:glycerol ratio on conversion and product selectivity over Mo/SiO_2 at 325 °C. Reaction conditions: 60 wt % glycerol/H_2O, 3 mL catalyst bed, 60 bar H_2. Other products: acetol, methane, ethane, propane, CO, CO_2, unknowns. c) Effect of H_2:glycerol ratio on conversion and product selectivity over W/Al_2O_3 at 325 °C. Reaction conditions: 60 wt % glycerol/H_2O, 3 mL catalyst bed, 60 bar H_2. Other products: acetol, methane, ethane, propane, CO, CO_2, unknowns. d) Effect of H_2:glycerol ratio on conversion and product selectivity over W/SiO_2 at 325 °C. Reaction conditions: 60 wt % glycerol/H_2O, 3 mL catalyst bed, 60 bar H_2. Other products: acetol, methane, ethane, propane, CO, CO_2, unknowns.

followed by readsorption onto the support via the primary hydroxyl groups of this intermediate to generate 3-hydroxypropene. Subsequently 3-HPA is formed via keto−enol tautomerization and undergoes quick hydrogenation on the active metal sites under hydrogen to yield 1,3-PDO. The fast hydrogenation of 3-HPA is important to prevent further dehydration of 3-HPA to produce acrolein. The higher selectivity to 1,2-PDO over Mo/Al_2O_3 might be related to this catalyst being relatively less active in converting this intermediate as compared to the other catalysts presented in

this study. The longest recorded performance of these catalysts was for 24 h at 325 °C, and there was no observable change in glycerol conversion and product distribution.

The total selectivity to monoalcohols (methanol, ethanol, 2-propanol, 1-propanol) was 34.6, 64.8, 70.6 and 54.6% over Mo/ Al_2O_3, Mo/SiO_2, W/Al_2O_3, and W/SiO_2 respectively. The selectivity to lower alcohols over Mo/Al_2O_3 was the lowest, likely due to the poor conversion of 1,2-PDO, which was the lowest among the catalysts. The selectivity to 1-propanol over Mo/SiO_2 at the highest temperature is consistent with results obtained by Shinmi et al.[31] and Koso et al.,[12] who found the highest 1-propanol selectivity, among the monoalcohols, over Rh−Mo/SiO_2 catalysts. Under similar reaction conditions, a glycerol conversion of 96.1 and 99.9% over Ni/Al_2O_3 and Ni/ SiO_2 respectively has been reported.[7] The total selectivity to monoalcohols was 54.5 and 68.5% over Ni/Al_2O_3 and Ni/SiO_2 respectively. Of other base metal catalysts that have been reported, Cu catalysts have been shown to give a high selectivity to 1,2-PDO (>90%), while Co and Ni tend to form EG and ethanol due to their affinity for C−C bond cleavage.[69−71] At lower temperature and pressure, some supported W catalysts have been reported to be selective to 1,3-PDO.[28, 72] Zhu et al.[27] more recently reported a glycerol conversion of 66.1% and a selectivity to 1,3-PDO as high as 66.1%.

Effect of H_2:Glycerol Ratio. Figures 6a−6d show the effect of the H_2:glycerol ratio on the conversion and product selectivity over the supported Mo and W catalysts at 325 °C. An increase in hydrogen content led to an increase in the conversion over all catalysts, and this is also in agreement with the calculated turnover frequencies in Table S1. It also led to an increase in selectivity to the lower alcohols, 73.6, 72.8, 85.3, and 66.1% over Mo/Al_2O_3, Mo/SiO_2, W/Al_2O_3, and W/SiO_2 respectively, when the H_2:glycerol ratio was 2:1. The total lower alcohol selectivity obtained over W/Al_2O_3 was remarkable, and, to our knowledge, such high selectivity has not been reported previously. The selectivity to 1,2-PDO was found to decrease due to the subsequent formation of lower alcohols such as ethanol (6−23%) and 1-propanol (15−33%). Due to the affinity of Mo catalysts to C−C bond cleavage, the selectivity to EG over these catalysts increased due to bond cleavage of glycerol. The selectivity to methanol was also much higher over both Mo and W catalysts due to simultaneous C−C bond cleavage of both EG and ethanol.

CONCLUSIONS

In conclusion, the activity of the catalysts was related to their Brønsted acidity, where an increase in acidity led to an increase in the glycerol conversion to as high as 73% over W/Al_2O_3. At 325 °C, the highest selectivity to the lower alcohols was also obtained; 34.6, 64.8, 70.6, and 54.6% over Mo/Al_2O_3, Mo/ SiO_2, W/Al_2O_3, and W/SiO_2 respectively. Doubling the H_2:glycerol ratio enhanced the activity of all catalysts, with it being almost double over Mo/SiO_2. The total selectivity to lower alcohols also increased to 73.6, 72.8, and 66.1% over Mo/ Al_2O_3, Mo/SiO_2, and W/SiO_2 respectively and a remarkable 85.3% over W/Al_2O_3.

ASSOCIATED CONTENT

* Supporting Information

The Supporting Information is available free of charge on the ACS Publications website at DOI: 10.1021/acssuschemeng.6b01675.

TPD profiles, Raman spectra, W(4f) and Mo(3d) XPS and TEM images of the Mo and W catalysts, and table of TOF results of Mo and W catalysts at various temperatures and H_2:glycerol ratios (PDF)

AUTHOR INFORMATION

Corresponding Author

*E-mail: friedric@ukzn.ac.za.

Notes

The authors declare no competing financial interest.

ACKNOWLEDGMENTS

The authors would like to thank the National Research Foundation and Technology and Human Resources for Industry Programme for financial support, the Microscopy and Microanalysis Unit (University of KwaZulu-Natal) for TEM analysis, Sasol Technology R&T for TPR and TPD analysis, and the Cardiff Catalysis Institute for XPS analysis.

REFERENCES

(1) Zhou, C.-H.; Beltramini, J. N.; Fan, Y.-X.; Lu, G. Q. Chemoselective catalytic conversion of glycerol as a biorenewable source to valuable commodity chemicals. Chem. Soc. Rev. 2008, 37, 527−549.

(2) Ota, N.; Tamura, M.; Nakagawa, Y.; Okumura, K.; Tomishige, K. Performance, Structure, and Mechanism of ReO_x−Pd/CeO_2 Catalyst for Simultaneous Removal of Vicinal OH Groups with H_2. ACS Catal. 2016, 6, 3213−3226.

(3) Rahmat, N.; Abdullah, A. Z.; Mohamed, A. R. Recent progress on innovative and potential technologies for glycerol transformation into fuel additives: A critical review. Renewable Sustainable Energy Rev. 2010, 14, 987−1000.

(4) Amada, Y.; Ota, N.; Tamura, M.; Nakagawa, Y.; Tomishige, K. Selective Hydrodeoxygenation of Cyclic Vicinal Diols to Cyclic Alcohols over Tungsten Oxide−Palladium Catalysts. ChemSusChem 2014, 7, 2185−2192.

(5) Miyazawa, T.; Koso, S.; Kunimori, K.; Tomishige, K. Development of a Ru/C catalyst for glycerol hydrogenolysis in combination with an ion-exchange resin. Appl. Catal., A 2007, 318, 244−251.

(6) Miyazawa, T.; Kusunoki, Y.; Kunimori, K.; Tomishige, K. Glycerol conversion in the aqueous solution under hydrogen over Ru/ C + an ion-exchange resin and its reaction mechanism. J. Catal. 2006, 240, 213−221.

(7) Van Ryneveld, E.; Mahomed, A. S.; van Heerden, P. S.; Green, M. J.; Friedrich, H. B. A catalytic route to lower alcohols from glycerol using Ni-supported catalysts. Green Chem. 2011, 13, 1819−1827.

(8) Amada, Y.; Koso, S.; Nakagawa, Y.; Tomishige, K. Hydrogenolysis of 1,2-Propanediol for the Production of Biopropanols from Glycerol. ChemSusChem 2010, 3, 728−736.

(9) Sun, D.; Yamada, Y.; Sato, S.; Ueda, W. Glycerol hydrogenolysis into useful C3 chemicals. Appl. Catal., B 2016, 193, 75−92.

(10) García-Fernandez, S.; Gandarias, I.; Requies, J.; Güemez, M. B.; Bennici, S.; Auroux, A.; Arias, P. L. New approaches to the Pt/WO_x/ Al_2O_3 catalytic system behavior for the selective glycerol hydro-genolysis to 1,3-propanediol. J. Catal. 2015, 323, 65−75.

(11) Liu, L.; Zhang, Y.; Wang, A.; Zhang, T. Mesoporous WO_3 Supported Pt Catalyst for Hydrogenolysis of Glycerol to 1,3-Propanediol. Chin. J. Catal. 2012, 33, 1257−1261.

(12) Koso, S.; Watanabe, H.; Okumura, K.; Nakagawa, Y.; Tomishige, K. Comparative study of Rh−MoO_x and Rh−ReO_x supported on SiO_2 for the hydrogenolysis of ethers and polyols. Appl. Catal., B 2012, 111−112, 27−37.

(13) Liao, X.; Li, K.; Xiang, X.; Wang, S.; She, X.; Zhu, Y.; Li, Y. Mediatory role of K, Cu and Mo over Ru/SiO_2 catalysts for glycerol hydrogenolysis. J. Ind. Eng. Chem. 2012, 18, 818−821.

(14) Tamura, M.; Amada, Y.; Liu, S.; Yuan, Z.; Nakagawa, Y.; Tomishige, K. Promoting effect of Ru on Ir-ReO_x/SiO_2 catalyst in hydrogenolysis of glycerol. J. Mol. Catal. A: Chem. 2014, 388−389, 177−187.

(15) Ota, N.; Tamura, M.; Nakagawa, Y.; Okumura, K.; Tomishige, K. Hydrodeoxygenation of Vicinal OH Groups over Heterogeneous Rhenium Catalyst Promoted by Palladium and Ceria Support. Angew. Chem. 2015, 127, 1917−1920.

(16) Nakagawa, Y.; Shinmi, Y.; Koso, S.; Tomishige, K. Direct hydrogenolysis of glycerol into 1,3-propanediol over rhenium-modified iridium catalyst. J. Catal. 2010, 272, 191−194.

(17) Amada, Y.; Shinmi, Y.; Koso, S.; Kubota, T.; Nakagawa, Y.; Tomishige, K. Reaction mechanism of the glycerol hydrogenolysis to 1,3-propanediol over Ir−ReO_x/SiO_2 catalyst. Appl. Catal., B 2011, 105, 117−127.

(18) Nakagawa, Y.; Ning, X.; Amada, Y.; Tomishige, K. Solid acid co-catalyst for the hydrogenolysis of glycerol to 1,3-propanediol over Ir-ReO_x/SiO_2. Appl. Catal., A 2012, 433−434, 128−134.

(19) Kurosaka, T.; Maruyama, H.; Naribayashi, I.; Sasaki, Y. Production of 1,3-propanediol by hydrogenolysis of glycerol catalyzed by Pt/WO_3/ZrO_2. Catal. Commun. 2008, 9, 1360−1363.

(20) Gong, L.; Lu, Y.; Ding, Y.; Lin, R.; Li, J.; Dong, W.; Wang, T.; Chen, W. Selective hydrogenolysis of glycerol to 1,3-propanediol over a Pt/$WO_3/TiO_2/SiO_2$ catalyst in aqueous media. Appl. Catal., A 2010, 390, 119−126.

(21) Zhu, S.; Zhu, Y.; Hao, S.; Zheng, H.; Mo, T.; Li, Y. One-step Hydrogenolysis of Glycerol to Biopropanols over Pt-$H_4SiW_{12}O_{40}$/ZrO_2 Catalysts. Green Chem. 2012, 14, 2607−2616.

(22) Zhu, S.; Qiu, Y.; Zhu, Y.; Hao, S.; Zheng, H.; Li, Y. Hydrogenolysis of glycerol to 1,3-propanediol over bifunctional catalysts containing Pt and heteropolyacids. Catal. Today 2013, 212, 120−126.

(23) Zhu, S.; Gao, X.; Zhu, Y.; Zhu, Y.; Xiang, X.; Hu, C.; Li, Y. Alkaline metals modified Pt−$H_4SiW_{12}O_{40}/ZrO_2$ catalysts for the selective hydrogenolysis of glycerol to 1,3-propanediol. Appl. Catal., B 2013, 140−141, 60−67.

(24) Arundhathi, R.; Mizugaki, T.; Mitsudome, T.; Jitsukawa, K.; Kaneda, K. Highly Selective Hydrogenolysis of Glycerol to 1,3-Propanediol over a Boehmite-Supported Platinum/Tungsten Catalyst. ChemSusChem 2013, 6, 1345−1347.

(25) Zhang, Y.; Zhao, X.; Wang, Y.; Zhou, L.; Zhang, J.; Wang, J.; Wang, A.; Zhang, T. Mesoporous Ti−W oxide: synthesis, character-ization, and performance in selective hydrogenolysis of glycerol. J. Mater. Chem. A 2013, 1, 3724−3732.

(26) Nakagawa, Y.; Tamura, M.; Tomishige, K. Catalytic materials for the hydrogenolysis of glycerol to 1,3-propanediol. J. Mater. Chem. A 2014, 2, 6688−6702.

(27) Zhu, S.; Gao, X.; Zhu, Y.; Li, Y. Promoting effect of WOx on selective hydrogenolysis of glycerol to 1,3-propanediol over bifunc-tional Pt−WO_x/Al_2O_3 catalysts. J. Mol. Catal. A: Chem. 2015, 398, 391−398.

(28) Zhu, S.; Gao, X.; Zhu, Y.; Cui, J.; Zheng, H.; Li, Y. SiO_2 promoted Pt/WO_x/ZrO_2 catalysts for the selective hydrogenolysis of glycerol to 1,3-propanediol. Appl. Catal., B 2014, 158−159, 391−399.

(29) Zhu, S.; Zhu, Y.; Hao, S.; Chen, L.; Zhang, B.; Li, Y. Aqueous-Phase Hydrogenolysis of Glycerol to 1,3-propanediol Over Pt-$H_4SiW_{12}O_{40}/SiO_2$. Catal. Lett. 2012, 142, 267−274.

(30) Shimao, A.; Koso, S.; Ueda, N.; Shinmi, Y.; Furikado, I.; Tomishige, K. Promoting Effect of Re Addition to Rh/SiO_2 on Glycerol Hydrogenolysis. Chem. Lett. 2009, 38, 540−541.

(31) Shinmi, Y.; Koso, S.; Kubota, T.; Nakagawa, Y.; Tomishige, K. Modification of Rh/SiO_2 catalyst for the hydrogenolysis of glycerol in water. Appl. Catal., B 2010, 94, 318−326.

(32) Yoneyama, Y.; Song, C. A new method for preparing highly active unsupported Mo sulfide. Catalytic activity for hydrogenolysis of 4-(1-naphthylmethyl)bibenzyl. Catal. Today 1999, 50, 19−27.

(33) Borowiecki, T.; Giecko, G.; Panczyk, M. Effects of small MoO3 additions on the properties of nickel catalysts for the steam reforming of hydrocarbons: II. Ni-Mo/Al_2O_3 catalysts in reforming, hydrogenolysis and cracking of n-butane. Appl. Catal., A 2002, 230, 85−97.

(34) Borowiecki, T.; Dziembaj, R.; Drozdek, M.; Giecko, G.; Panczyk, M.; Piwowarska, Z. Studies of the model Ni-Mo/alumina catalysts in the n-butane reaction hydrogenolysis. Appl. Catal., A 2003, 247, 17−25.

(35) Koso, S.; Ueda, N.; Shinmi, Y.; Okumura, K.; Kizuka, T.; Tomishige, K. Promoting effect of Mo on the hydrogenolysis of tetrahydrofurfuryl alcohol to 1,5-pentanediol over Rh/SiO_2. J. Catal. 2009, 267, 89−92.

(36) van Ryneveld, E.; Mahomed, A. S.; van Heerden, P. S.; Friedrich, H. B. Direct Hydrogenolysis of Highly Concentrated Glycerol Solutions Over Supported Ru, Pd and Pt Catalyst Systems. Catal. Lett. 2011, 141, 958−967.

(37) Zhou, J.; Xu, N. S.; Deng, S. Z.; Chen, J.; She, J. C.; Wang, Z. L. Large-Area Nanowire Arrays of Molybdenum and Molybdenum Oxides: Synthesis and Field Emission Properties. Adv. Mater. 2003, 15, 1835−1840.

(38) Senthil, K.; Yong, K. Growth and characterization of stoichiometric tungsten oxide nanorods by thermal evaporation and subsequent annealing. Nanotechnology 2007, 18, 395604.

(39) Imamoglu, Y.; Zumreoglu-Karan, B.; Amass, A. J. Olefin Metathesis and Polymerization Catalysts; Springer: Netherlands, 1990.

(40) Lopez-Suarez, F. E.; Parres-Esclapez, S.; Bueno-Lopez, A.; Illan-Gomez, M. J.; Ura, B.; Trawczynski, J. Role of surface and lattice copper species in copper-containing (Mg/Sr)TiO_3 perovskite catalysts for soot combustion. Appl. Catal., B 2009, 93, 82−89.

(41) Aleman-Vazquez, L. O.; Hernandez-Perez, F.; Cano-Domínguez, J. L.; Rodríguez-Hernandez, A.; García-Gutierrez, J. L. Binder effect on the catalytic activity of MoO_3 bulk catalyst reduced by H_2 for n-heptane hydroisomerization. Fuel 2014, 117, 463−469.

(42) Saghafi, M.; Heshmati-Manesh, S.; Ataie, A.; Khodadadi, A. A. Synthesis of nanocrystalline molybdenum by hydrogen reduction of mechanically activated MoO_3. Int. J. Refract. Hard Met. 2012, 30, 128− 132.

(43) Jia, Y.; Li, G.; Ning, G. Efficient oxidative desulfurization (ODS) of model fuel with H_2O_2 catalyzed by MoO_3/γ-Al_2O_3 under mild and solvent free conditions. Fuel Process. Technol. 2011, 92, 106−111.

(44) Wang, B.; Ding, G.; Shang, Y.; Lv, J.; Wang, H.; Wang, E.; Li, Z.; Ma, X.; Qin, S.; Sun, Q. Effects of MoO_3 loading and calcination temperature on the activity of the sulphur-resistant methanation catalyst MoO_3/γ-Al_2O_3. Appl. Catal., A 2012, 431-432, 144−150.

(45) Braun, S.; Appel, L. G.; Schmal, M. Molybdenum species on alumina and silica supports for soot combustion. Catal. Commun. 2005, 6, 7−12.

(46) Falco, M. G.; Canavese, S. A.; Fígoli, N. S. Preparation of tungsten oxide promoted zirconia by different methods. Catal. Today 2005, 107-108, 778−784.

(47) Wachs, I. E.; Kim, T.; Ross, E. I. Catalysis science of the solid acidity of model supported tungsten oxide catalysts. Catal. Today 2006, 116, 162−168.

(48) Vermaire, D. C.; van Berge, P. C. The preparation of WO_3TiO_2 and $WO_3Al_2O_3$ and characterization by temperature-programmed reduction. J. Catal. 1989, 116, 309−317.

(49) Horsley, J. A.; Wachs, I. E.; Brown, J. M.; Via, G. H.; Hardcastle, F. D. Structure of surface tungsten oxide species in the tungsten trioxide/alumina supported oxide system from x-ray absorption near-edge spectroscopy and Raman spectroscopy. J. Phys. Chem. 1987, 91, 4014−4020.

(50) Chen, K.; Xie, S.; Bell, A. T.; Iglesia, E. Structure and Properties of Oxidative Dehydrogenation Catalysts Based on MoO_3/Al_2O_3. J. Catal. 2001, 198, 232−242.

(51) Kitano, T.; Okazaki, S.; Shishido, T.; Teramura, K.; Tanaka, T. Brønsted acid generation of alumina-supported molybdenum oxide calcined at high temperatures: Characterization by acid-catalyzed reactions and spectroscopic methods. J. Mol. Catal. A: Chem. 2013, 371, 21−28.

(52) Mitran, G.; Yuzhakova, T.; Popescu, I.; Marcu, I.-C. Study of the esterification reaction of acetic acid with n-butanol over supported WO_3 catalysts. J. Mol. Catal. A: Chem. 2015, 396, 275−281.
(53) Barton, D. G.; Soled, S. L.; Meitzner, G. D.; Fuentes, G. A.; Iglesia, E. Structural and Catalytic Characterization of Solid Acids Based on Zirconia Modified by Tungsten Oxide. J. Catal. 1999, 181, 57−72.
(54) Jeziorowski, H.; Knozinger, H.; Grange, P.; Gajardo, P. Raman-Spectra of Cobalt Molybdenum Oxide Supported on Silica. J. Phys. Chem. 1980, 84, 1825−1829.
(55) Rinaldi, N.; Kubota, T.; Okamoto, Y. Effect of citric acid addition on the hydrodesulfurization activity of MoO_3/Al_2O_3 catalysts. Appl. Catal., A 2010, 374, 228−236.
(56) Miao, Y.; Lu, G.; Liu, X.; Guo, Y.; Wang, Y.; Guo, Y. The molybdenum species of MoO_3/SiO_2 and their catalytic activities for the epoxidation of propylene with cumene hydroperoxide. J. Ind. Eng. Chem. 2010, 16, 45−50.
(57) Han, X.; Wang, A.; Wang, X.; Li, X.; Wang, Y.; Hu, Y. Catalytic performance of P-modified MoO_3/SiO_2 in oxidative desulfurization by cumene hydroperoxide. Catal. Commun. 2013, 42, 6−9.
(58) Adamiak, J.; Tomaszewski, W.; Skupinski, W. Interaction of nitromethane with MoO_3/SiO_2 and its influence on toluene nitration. Catal. Commun. 2012, 29, 92−95.
(59) Moraes, R.; Thomas, K.; Thomas, S.; Van Donk, S.; Grasso, G.; Gilson, J.; Houalla, M. Ring opening of decalin and methylcyclohexane over alumina-based monofunctional WO_3/Al_2O_3 and Ir/Al_2O_3 catalysts. J. Catal. 2012, 286, 62−77.
(60) Lu, G.; Li, X.; Wang, Y.; Chen, G.; Qu, Z. Selective oxidation of cyclopentene to glutaraldehyde over the WO_3/SiO_2 catalyst. Appl. Surf. Sci. 2008, 255, 3117−3120.
(61) Haneda, M.; Hamada, H. Promotional role of H_2O in the selective catalytic reduction of NO with CO over $Ir/WO_3/SiO_2$ catalyst. J. Catal. 2010, 273, 39−49.
(62) Uppachai, P.; Harnchana, V.; Pimanpang, S.; Amornkitbamrung, V.; Brown, A. P.; Brydson, R. M. D. A substoichiometric tungsten oxide catalyst provides a sustainable and efficient counter electrode for dye-sensitized solar cells. Electrochim. Acta 2014, 145, 27−33.
(63) Baltrusaitis, J.; Mendoza-Sanchez, B.; Fernandez, V.; Veenstra, R.; Dukstiene, N.; Roberts, A.; Fairley, N. Generalized molybdenum oxide surface chemical state XPS determination via informed amorphous sample model. Appl. Surf. Sci. 2015, 326, 151−161.
(64) Van Ryneveld, E.; Mahomed, A. S.; Van Heerden, P. S.; Green, M. J.; Holzapfel, C.; Friedrich, H. B. The selective continuous flow synthesis of lower alcohols from polyols − a mechanistic interpretation of the results. Catal. Sci. Technol. 2014, 4, 832−837.
(65) Ueda, N.; Nakagawa, Y.; Tomishige, K. Conversion of Glycerol to Ethylene Glycol over Pt-modified Ni Catalyst. Chem. Lett. 2010, 39, 506−507.
(66) Gandarias, I.; Arias, P. L.; Requies, J.; Gueemez, M. B.; Fierro, J. L. G. Hydrogenolysis of glycerol to propanediols over a Pt/ASA catalyst: The role of acid and metal sites on product selectivity and the reaction mechanism. Appl. Catal., B 2010, 97, 248−256.
(67) Miyazawa, T.; Kusunoki, Y.; Kunimori, K.; Tomishige, K. Glycerol conversion in the aqueous solution under hydrogen over Ru/ C + an ion-exchange resin and its reaction mechanism. J. Catal. 2006, 240, 213−221.
(68) Priya, S. S.; Bhanuchander, P.; Kumar, V. P.; Dumbre, D. K.; Periasamy, S. R.; Bhargava, S. K.; Lakshmi Kantam, M.; Chary, K. V. R. Platinum Supported on H-Mordenite: A Highly Efficient Catalyst for Selective Hydrogenolysis of Glycerol to 1,3-Propanediol. ACS Sustainable Chem. Eng. 2016, 4, 1212−1222.
(69) Guo, X.; Li, Y.; Song, W.; Shen, W. Glycerol Hydrogenolysis over Co Catalysts Derived from a Layered Double Hydroxide Precursor. Catal. Lett. 2011, 141, 1458−1463.
(70) Perosa, A.; Tundo, P. Selective Hydrogenolysis of Glycerol with Raney Nickel. Ind. Eng. Chem. Res. 2005, 44, 8535−8537.
(71) Hirunsit, P.; Luadthong, C.; Faungnawakij, K. Effect of alumina hydroxylation on glycerol hydrogenolysis to 1,2-propanediol over Cu/Al_2O_3: combined experiment and DFT investigation. RSC Adv. 2015, 5, 11188−11197.
(72) Qin, L.-Z.; Song, M.-J.; Chen, C.-L. Aqueous-phase deoxygenation of glycerol to 1,3-propanediol over $Pt/WO_3/ZrO_2$ catalysts in a fixed-bed reactor. Green Chem. 2010, 12, 1466−1472.